# Contingency Path Planning for Hybrid-electric UAS

Anthony Reinier Hovenburg[1,2], Fabio Augusto de Alcantara Andrade[1,3,4], Christopher Dahlin Rodin[1,2], Tor Arne Johansen[1] and Rune Storvold[1,3]

***Abstract*— This article presents a path planning optimization method which aims to mitigate the risks in the event of a critical engine or generator failure in hybrid-electric UAS. This is achieved through continuous determination of the optimum flight path, based on the remaining battery range and expected local wind conditions. The result is a dynamically adjusting flight path which ensures the aircraft to remain within range of pre-specified safe landing spots. The developed algorithm uses the particle swarm optimization technique to optimize the flight path, and incorporates regional wind information in order to increase the accuracy of the expected in-flight performance of the aircraft.**

## I. Introduction

Hybrid-electric power trains used by long-range fixed-wing unmanned aerial vehicles often employ an internal combustion engine as the main source of power. It is witnessed that the internal combustion engine often is a critical point of failure. In such an event a functioning electric motor may still be able to propel the aircraft for a short period by utilizing the remaining battery capacity.

In an effort to contribute to the current scientific search towards path safety within autonomous decision-making, this paper proposes a new method for contingent path planning optimization. The main goal of this study is to derive a method for autonomous path planning which ensures that the aircraft is able to reach a safe landing spot in the event of a critical engine or generator failure. This is done while taking into consideration the presence of expected local winds and their effect on the obtainable battery range. The resulting optimum path is found by applying the technique of Particle Swarm Optimization (PSO) [1].

In recent scientific literature path planning algorithm methods are described which use local wind information. In [2], the author integrates the uncertainty of the wind field into the wind model, and uses a Markov Decision Process for path planning. The goal was to minimize the power consumption of the aircraft and minimize time-to-goal. A similar approach was chosen in [3], where the technique of Ant Colony Optimization (ACO) is used to find the path which minimizes the travel time considering the wind. However, as with most studies the wind is considered constant during the flight. The ACO is a bio-inspired metaheuristic optimization algorithm suchlike the Particle Swarm Optimization used in this study. PSO is widely used for path planning, such as described in [4], where the author uses the method to minimize the UAS path's length and danger based on the proximity of threats.

The study presented in this paper builds further upon the before mentioned methods by incorporating a dynamic wind model and translating this into the real-time in-flight performance of hybrid-electric UAS.

## II. Aircraft performance model

The resulting achievable flight range is described in the following subsections. This is illustrated by analyzing the different segments of a flight that suffers a critical engine or generator failure. The flight segments are divided into normal operations, battery-powered flight, and unpowered glide.

### A. Aircraft Power Model

For a conventional propeller-driven aircraft in level and unaccelerated flight, the power that is required for obtaining the maximum flight range is expressed, in watts, by:

$$P_{rmr} = W \left( \frac{C_D}{C_L} \right)_{min} \cdot v_{TAS} \tag{1}$$

where $W$ is the aircraft total weight in Newton, $(C_D/C_L)_{min}$ is the minimum obtainable ratio between the aerodynamic drag and lift coefficients, and $v_{TAS}$ is the true airspeed occurring at the $(C_D/C_L)_{min}$ condition.

One advantage of utilizing a hybrid-electric power train is that there is the possibility of co-powering the main drive shaft (continuous or intermittent). Depending on the sizing of the hybrid system and mission specifications, this may prove to be beneficial for the resulting range. A method for determining the achievable range in the case of co-powering of a hybrid system is described by Marwa in [5]. In the remainder of this analytical study it is further assumed that a functioning main generator set is sized so that it is capable of supplying the necessary power required for maintaining the maximum range cruise speed ($v_{mr}$). Therefore during cruise it is given that the necessary amount of co-powering by the electric motor is zero.

### B. Aircraft range - Normal operations

In the case of a hybrid powered aircraft where the electric co-powering equals zero, the obtainable maximum range may be modelled similarly to conventional fuel-powered aircraft. The Breguet range equation is a commonly used first-order approximation to determine the achievable maximum range of a conventional propeller aircraft [6]. When assuming no wind and a parabolic drag polar, the resulting maximum

[1]NTNU Centre for Autonomous Marine Operations and System, Department of Engineering Cybernetics, Norwegian University of Science and Technology, Trondheim, Norway

[2]Maritime Robotics A/S, Trondheim, Norway

[3]NORUT Northern Research Institute, Tromsø, Norway

[4]CEFET/RJ Federal Center of Technological Education of Rio de Janeiro, Rio de Janeiro, Brazil

range in normal operations ($R_{no}$ in meters) is expressed by [7]:

$$R_{no} = \frac{\eta_{pg}}{c} \cdot \left(\frac{C_L}{C_D}\right)_{max} \cdot ln\left(\frac{W_0}{W_1}\right) \tag{2}$$

where $\eta_{pg}$ is the complete propulsion efficiency of the hybrid system, $c$ is the specific fuel consumption of the generator in Newtons per second per Watt, $W_0$ is the aircraft's total weight at the beginning of the cruise flight, $W_1$ is the aircraft's total weight at the end of the cruise flight, and $(C_L/C_D)_{max}$ is the maximum achievable ratio between the aerodynamic lift and drag coefficients in level and unaccelerated flight.

### C. Aircraft range - Battery-powered flight

In a situation where the main engine or generator fails, the hybrid system remains able to supply the power necessary to propel the aircraft by utilizing the remaining battery capacity. To obtain the performance model the aircraft is considered purely battery-powered. The adopted method for determining the maximum achievable range of battery-powered sUAS has previously been described in [8]. The adopted method in that study is an extension on the classical determination of battery-powered aircraft range, by including the Peukert effect on the battery capacity. This allows for a more accurate determination of the aircraft's battery range [9][10]. When assuming no wind and a parabolic drag polar, the maximum range ($R_{bp}$, in kilometers) for battery-powered sUAS in level and unaccelerated flight, without the influence of wind, is expressed by:

$$R_{bp} = \left(\frac{V \times C\,\eta_{pe}}{W\left(\frac{C_D}{C_L}\right)_{min}}\right)^{n} \left(\sqrt{\frac{2W}{\rho_\infty\, S\, C_L}}\right)^{1-n} \cdot {R_t}^{1-n} \cdot 3.6 \tag{3}$$

Here $V$ is the battery bus voltage, $C$ is the battery capacity, $n$ is the battery-specific Peukert constant, $R_t$ is the battery hour rating (i.e. the discharge period at which the rated capacity $C$ was determined), and $\eta_{pe}$ is the propulsion efficiency of the battery-powered system. The amount of experienced resistance depends on the specific set-up, and the availability of mitigation systems, such as mechanical decoupling.

### D. Aircraft range - Unpowered glide

After the main batteries have been drained, the aircraft may be able to fly further by exchanging its altitude for range. This flight phase is modelled as pure unpowered glide, depending solely on the altitude ($h$), and maximum glide ratio $(L/D)_{max}$. When the aircraft's glide angle is moderate the maximum range for unpowered glide in no-wind condition and for flat terrain is expressed by [11]:

$$R_{ug} = h\left(\frac{L}{D}\right)_{max} \tag{4}$$

### E. Effects of Wind

Small unmanned aircraft are often operating in relatively high wind speeds - commonly exceeding half of the true air speed. Depending on the speed and direction, en-route winds may have a significant influence on the obtainable range of the aircraft. Therefore, in an effort to accurately estimate the maximum obtainable range of an aircraft, one has to include the wind effects. This study aims to describes a method for determining the maximum obtainable range, while including the effects of horizontal winds that are encountered en-route. Note that this wind model shall be applied to each segment of the flight.

In [12] it is described how the optimum airspeed may be determined when accounting for head- and tailwinds. The author states that for propeller-powered aircraft the optimum airspeed is obtained through:

$$m_{br} = \frac{v_{TAS}}{v_{br}} = \left[\frac{2\,m_{br} \pm \left(\frac{v_w}{v_{md}}\right)}{2\,m_{br} \pm 3\left(\frac{v_w}{v_{md}}\right)}\right]^{\frac{1}{4}} \tag{5}$$

Here $m_{br}$ is the relative airspeed parameter between the true airspeed and the best-range airspeed ($v_{br}$). $v_w$ is the wind speed, with $\pm$ indicating a head- or tailwind, $v_{md}$ is the minimum-drag airspeed. Solving for $m_{br}$ yields the optimum ratio to achieve the best range in the event of head- or tailwind. As Eq. (5) only takes into account head- or tailwinds along the flight path, it is necessary to include and isolate the crosswind component that may be encountered en-route. When assuming a flat and non-rotating Earth and flying in level and unaccelerated flight, the equations of motion through decomposed wind vectors are modelled as:

$$v_{GS} = v_{TAS} \begin{bmatrix} cos\,\phi \\ sin\,\phi \end{bmatrix} + v_w \begin{bmatrix} cos\,\theta_w \\ sin\,\theta_w \end{bmatrix} \tag{6}$$

Here $v_{GS}$ is the aircraft's ground velocity vector, and $\theta_w$ is the direction of the wind. The aircraft's commanded heading ($\phi$) is the sum of the course angle ($\theta$) and the crab angle ($\beta$). Here $\beta$ is defined as the angle between the TAS vector and the ground course angle. The wind components perpendicular and parallel to the resulting ground track, in relation to the reference horizontal path, can be found by rotating the wind's x and y components through angle $\theta$, resulting in [13]:

$$\begin{aligned} v_{\parallel} &= v_{wN}\,\cos\,\theta + v_{wE}\,\sin\theta \\ v_{\perp} &= -v_{wN}\,\sin\,\theta + v_{wE}\,\cos\theta \end{aligned} \tag{7}$$

Considering the horizontal wind field to be described in the NED (North, East, Down) frame, then $v_{wE}$ is the decomposed East wind component, and $v_{wN}$ is the decomposed North wind component. $v_{\parallel}$ is the wind component parallel to the aircraft's ground course and $v_{\perp}$ is the perpendicular wind component to the ground course. In relation to Eq. (5) the parallel wind component constitutes the value for $v_w$.

## III. Path Planning

In this section, the optimization problem formulation and the cost function that has to be minimized by the Particle Swarm Optimization (PSO) are presented.

### A. Optimization Problem Formulation

In this study the goal is to find a safe path with the shortest length. Therefore, the cost function ought to take into consideration both the path's length and the safety. Here a safe path is defined as a path in which the aircraft, in the event of a critical engine or generator failure, is within flight range of a pre-specified safe landing spot.

A two-dimensions geographical approach is used in this work, where the optimization variables represent a set of waypoints of the path, with $x$ (North) and $y$ (East) positions in the NED frame. As the input positions of the origin, destination and landings spots are given in latitude and longitude coordinates, a conversion to the NED frame is needed. Besides, to use the result as an input for an Autopilot system it may be required to convert the waypoints to positions expressed in latitude and longitude.

The domain has to be defined taking into consideration that the UAV may not deviate too far from the straight line path between the departure and destination. To initialize the optimization algorithm, first a straight path from the origin to the destination is generated - with waypoints distributed equally along the path. This strategy is crucial, as usually the optimal solution will be a deviation from this straight path. If only particles initialized with random positions are used, they might have uncommon waypoints displacement, causing the algorithm to take a long time to find an optimal solution or to get stuck in a local minimum.

The stop criteria used is straight forward. The algorithm runs until it reaches a pre-defined number of iterations.

### B. Cost Function

Always flying within range of a safe landing spot may not always be desired (or realistic), since this may cause the path to be too long. For that reason a cost function ($f$) is proposed that employs a method for weighing the importance of the safety against the importance of the path length. As shown in the following equation, $\alpha$ represents the weight of the path's length over the safety. This results in:

$$f = (\alpha)\, \textit{length} + (1-\alpha)\frac{1}{\textit{safety}} \tag{8}$$

Where *length* and *safety* are relative values and in this study presented as percentages. The function is calculated based on the minimum length, which is the straight line between the departure and destination, as per Eq. (9), and the maximum safety, if all points along the path are safe, as per Eq. (10).

$$\textit{length} = \frac{\text{current length } (L_{cur})}{\text{minimum length } (L_{min})} \tag{9}$$

$$\textit{safety} = \frac{\text{number of safe points } (n_{safe})}{\text{total number of points } (N_{path})} \tag{10}$$

To ensure that the safety is evaluated for the entire path, and not only for the position of the waypoint, an interpolation is performed to discretize the path into $N_{path}$ number of points. The effective flight range using battery power is calculated to all landing spots that are not further than the maximum range which the UAV could fly by taking into consideration a vector of wind that would provide the maximum range, thus, landing spots very far away are not considered in that step of the algorithm. As the wind might change along the path between the point and the landing spot, the range is recalculated every $R_{step}$ considering the closest wind vector.

For each point ($n$), it is evaluated if it is close enough to at least one landing spot ($j$). Then one unity is added to the safety result variable, demonstrated by:

$$n_{safe} = \sum_{n=1}^{N_{path}} \begin{cases} 1 & \text{if } (r_1^n < d_1)||...||(r_j^n < d_j) \\ 0 & \text{otherwise} \end{cases} \tag{11}$$

The total length is the sum of the distance between the points of the interpolation:

$$L_{cur} = \sum_{n=1}^{N_{path}} \sqrt{(x_n - x_{n-1})^2 + (y_n - y_{n-1})^2} \tag{12}$$

## IV. Case study and Experimental setup

### A. Case Study

The scenario chosen for this simulation comprises the area located to the north of the Norwegian city of Trondheim (fig. 1). For this study the Norwegian Defence Research Establishment (FFI) made regional wind models available for calculating wind speeds and directions for different altitudes with the resolution of 2.5 km. The date of the data retrieval was July 5th 2017, with wind information valid between 03:00PM and 09:00PM of that day. The orange polygon in the figure illustrates for which region the information was available. The locations of the origin (A) and destination (B) were chosen so that the maximum length across the wind model's specified area was utilized. The straight-line path distance between origin and destination is 210 kilometers, illustrated by the red dotted line, and has a path safety of 72.6%. The safe landing spot locations were manually selected through studying satellite imagery. The initial cruise altitude is chosen to be 1500 meters, meaning it can pass any mountain the aircraft may encounter within the specified region.

### B. Experimental Setup

This case study utilizes the P31015 concept UAV, which is a fixed-wing aircraft in conventional pusher configuration. In this theoretical study the model shall employ a hybrid propulsion system with sufficient capacity to allow continuous in-flight recharging of the batteries - effectively enabling fully charged batteries during cruise flight. The total propulsion efficiency through the generator ($\eta_{pg}$) is assumed to be invariable at 28.5% while the specific fuel

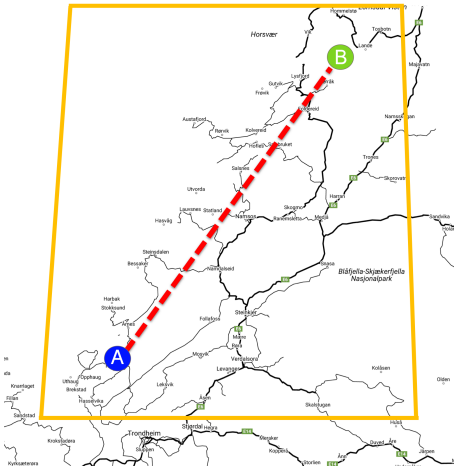


Fig. 1. Simulation scenario

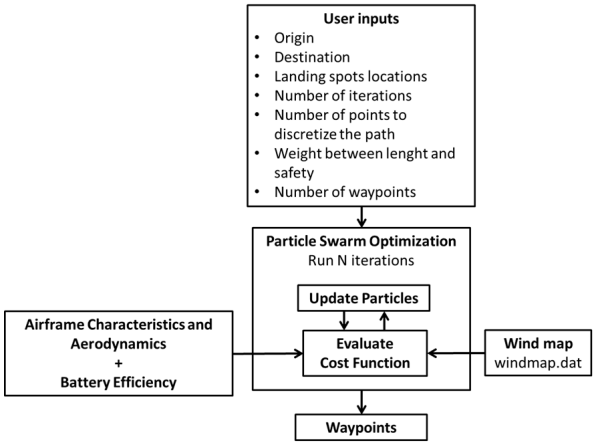


Fig. 2. Overall block diagram

consumption $c$ equals 383 grams per horsepower per hour. The direct electric propulsion efficiency ($\eta_{pe}$) is assumed to be invariable at 50%. These values lie within range of experimental data found in [9], [14] and [15]. At the initiation of the cruise phase the aircraft is modelled to carry 5.5 liters of on board fuel, and to have a fully charged battery with a usable nominal capacity of 10 Ampere-hours at 44.4 Volt. The total weight of the aircraft is assumed to be 17.5 kilograms. More detailed aircraft specifications may be found in [8].

The theoretical maximum obtainable range of the aircraft at any point in time during the cruise phase is calculated as the sum of $R_{no}$, $R_{mgf}$ and $R_{ug}$. As $R_{ug}$ is defined as the maximum obtainable range related to flat terrain, this requires to be re-evaluated when considering operating in mountainous terrain, such as the selected region for this experiment. The terrain in the selected region is mountainous, and contains elevated fields nearly as high as the selected cruise altitude. Therefore the actual obtainable glide range is considered too variant. Thus, in this specific simulation it is decided to leave out the potential range of unpowered glide, leaving the sum of $R_{no}$ and $R_{mgf}$ as the maximum obtainable range.

### C. MATLAB Code description

A MATLAB script was written to perform the simulation. The main user inputs are the WGS-84 coordinates of the origin, destination and safe landing spots. The wind information obtained was previously saved in a .mat file, which is used for the evaluation of the cost function. The airframe characteristics and battery efficiency, as detailed in previous sections, need to be configured. The optimization parameters are shown in the next subsection. The script is set up so that it runs the optimization algorithm until a pre-determined number of iterations is reached. Fig. 2 shows a simplified block diagram of the script.

### D. Parameters and Optimization Algorithm

Some parameters need to be defined in the optimization algorithm. Several of these parameters may strongly affect the convergence speed of the algorithm, and can prevent it from falling into local minima. Among these are the velocity constraint, which was chosen to be attached to the domain in order to be automatically changed according to the problem; and the initial and final inertia weight, which were chosen to range from 1.0 to 0.1, to allow a more global search at the beginning, and a more local search in the course of iterations. However, other parameters can hardly be modified as they are specified by the users requirements, which affects the processing time. For instance, this is the case with the number of points which discretize the path. The parameters used in this simulation are presented in the table below, where the domain is defined by $[x_{min}, x_{max}, y_{min}, y_{max}]$:

TABLE I
LIST OF PARAMETERS

| Name | Value |
|---|---|
| Number of iterations | 100 |
| Particle velocity constraint | 0.1 x Domain |
| $w_{ini}$ | 1.0 |
| $w_{fin}$ | 0.1 |
| $N_{steps}$ | 84 |
| Safe landing spots | 5 |
| $x_{min}$ | $x_s$-$L_{min}/2$ |
| $x_{max}$ | $x_t$+$L_{min}/2$ |
| $y_{min}$ | $y_s$-$L_{min}/2$ |
| $y_{max}$ | $y_t$+$L_{min}/2$ |
| $R_{step}$ | 5 km |

## V. RESULTS

Figure 3 shows the result in the NED frame for a simulation using $\alpha = 0.3$. The yellow square and the green star represent the origin and destination respectively. The red circles are the generated waypoints, while the red crosses represent the safe landing spots. The path's discretized points are presented as black dots. The arrows represent the distance

from the point of the path to a landing spot which the UAS can reach during a critical engine failure. This also takes into account the effects of wind. What may be observed is that the projected path is always close enough to safe landing spots (LS) 1, 2 or 5, resulting in LS2 and LS3 not being utilized within this scenario. It was found that in this specific scenario the calculated path has a safety factor of 100%, with a total length of 215.4 kilometers. This route is 5.4 kilometers longer than the straight path distance between origin and destination. The convergence of the algorithm is shown in Figure 4, where the vertical axis refers to the Cost Function, Eq. (8).

In an attempt to study the effects of the positioning and amount of safe landing spots, a second simulation was conducted where LS1 was removed, as illustrated in fig. 5. Here is it impossible to reach a safety score of 100% due to the distance between the landing spots. The grey line indicates the part of the path where the UAS cannot reach a landing spot in case of engine failure. In this specific case it was found that for $\alpha = 0.3$ the rated path safety was 83.3%, while the path distance had increased to 231.4 kilometers.

In a third scenario where five safe landing spots were placed at different locations, the simulation for $\alpha = 0.3$ resulted in a path with length 229.4 and safety of 100%.

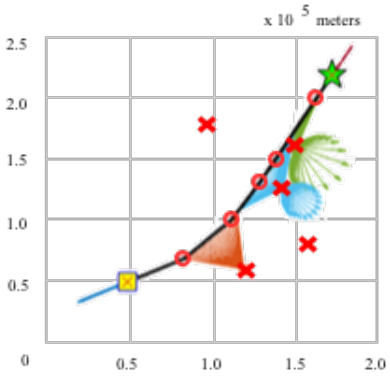


Fig. 3. Result for $\alpha = 0.3$

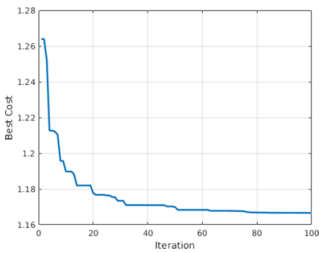


Fig. 4. Algorithm convergence

When $\alpha = 0.7$ was chosen, the length was shorter (219.9km), while the safety was 90.48%. Therefore in this scenario it was found that compared to the straight-line trajectory the trade-off made for $\alpha = 0.3$ is 27.4% increased safety against an increase of 19.4 kilometers in path length,

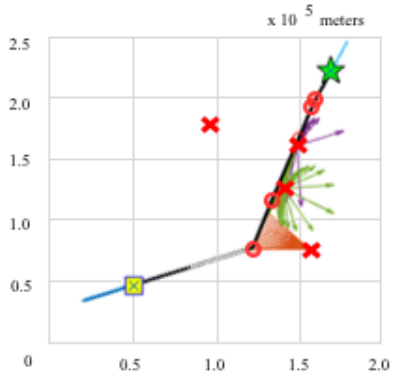


Fig. 5. Result without LS1 for $\alpha = 0.3$

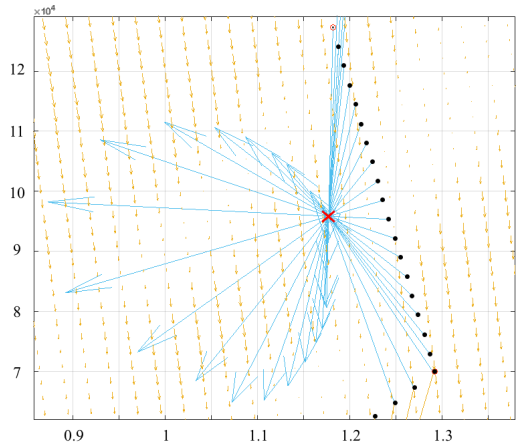


Fig. 6. Extract of path including the wind vectors

while for $\alpha = 0.7$ this is 17.9% increased safety against 9.9 kilometers increase in path length.

Fig. 6 illustrates a magnified part of the path, including the plotting of the wind vectors (orange arrows). The blue arrows represent by size the range that the UAS can obtain using the electrical battery from the discretized point of the path (black dots) to the landing spot (red cross). It may be observed that the wind is pointing south, resulting in a larger obtainable range when flying North to South, compared to flying South to North.

## VI. Limitations

The suggested methods are evaluated through performing simulations. The physical input parameters, such as the wind, are predicted values based on weather model simulations. The suggested method does not include vertical winds, nor was this information available. The aerodynamic and propulsion efficiency parameters that were used are drawn from a concept aircraft and hybrid system, with assumed performance characteristics. Although the geographic model is realistic, the safe landing spots were chosen arbitrarily. All before mentioned limitations may influence the accuracy of the proposed model, and therefore a verification of the model may be warranted.

## VII. Discussion and future work

To eliminate the limitations described in the previous section, and to further verify the proposed model, more simulations are needed. Besides the verification, a validation through flight test is to be conducted through utilizing an aircraft with known performance characteristics. In a future study the authors intend to optimize the algorithm's required calculating time, so that in-flight real-time recalculation becomes a possibility.

Though it is beyond the scope of this study, one might consider using a more sophisticated glide performance model, such as described in [16] which also includes the effects of turn performance on the achievable range, and consider [17] and [18] which describe an optimization method for the in-flight performance in variable (and altitude dependent) winds.

## VIII. Conclusion

In this paper a method was proposed that aims to increase the operational safety of hybrid-electric powered UAVs. This was done by taking into account the possibility of direct-electric propulsion in case of main generator failure. It was demonstrated that the aircraft's projected flight path can be adjusted so that it remains within range of pre-specified safe landing spots. This is done while taking into account the pre-calculated effects of winds that are encountered en-route by including an altitude-dependent wind model. As it is not always possible (or desirable) to have a completely safe path, the proposed method includes a cost function in which the user may specify the importance of path safety over the path length. A first simulation ($\alpha = 0.3$) with arbitrarily picked safe landing locations shows a path safety of 100%, while having a total path length of 215.4 kilometers. This is opposed to the straight path distance of 210.0 kilometers which offers a path safety of 72.6%. In this instance it is concluded that the trade-off may be an increased path safety of 27.4% at the cost of a longer path length of 5.4 kilometers. In a second simulation (also $\alpha = 0.3$) one central safe landing spot was removed. This simulation resulted in a weighed safe path of 83.3%, while having a total path length of 231.4 kilometers. The trade-off may be determined through a similar approach. A third scenario was tested where the five safe landing spots were placed at a different location, while $\alpha$ was chosen to be 0.3 and 0.7. In this scenario it was shown that compared to the straight-line trajectory the trade-off made for $\alpha = 0.3$ is 27.4% increased safety against an increase of 19.4 kilometers in path length, while for $\alpha = 0.7$ this is 17.9% increased safety against 9.9 kilometers increase in path length. The study presented here was a theoretical study based on simulations utilizing hypothetical aircraft systems. To further validate and verify the proposed methods, the authors suggest a future study with more diverse simulated scenarios, and to perform test flights conducted with an aircraft that has known performance characteristics.


## Acknowledgment

The authors want to thank the Norwegian Defence Research Establishement (FFI) for supplying the sophisticated local wind models that were used in this study.

This work has been supported by the MarineUAS project, funded by the European Comission under the H2020 Programme (MSCA-ITN-2014-642153). We also acknowledge the Research Council of Norway, grant number 223254 - Centre for Autonomous Marine Operations and Systems (NTNU-AMOS).


## References


[1] R. Eberhart and J. Kennedy, "A new optimizer using particle swarm theory," in *Micro Machine and Human Science, 1995. MHS'95., Proceedings of the Sixth International Symposium on*. IEEE, 1995, pp. 39–43.

[2] W. H. Al-Sabban, L. F. Gonzalez, and R. N. Smith, "Wind-energy based path planning for unmanned aerial vehicles using markov decision processes," in *Robotics and Automation (ICRA), 2013 IEEE International Conference on*. IEEE, 2013, pp. 784–789.

[3] A. L. Jennings, R. Ordonez, and N. Ceccarelli, "An ant colony optimization using training data applied to uav way point path planning in wind," in *Swarm Intelligence Symposium, 2008. SIS 2008. IEEE*. IEEE, 2008, pp. 1–8.

[4] S. Li, X. Sun, and Y. Xu, "Particle swarm optimization for route planning of unmanned aerial vehicles," in *Information Acquisition, 2006 IEEE International Conference on*. IEEE, 2006, pp. 1213–1218.

[5] M. Marwa, S. M. Martin, B. C. Martos, and R. P. Anderson, "Analytic and numeric forms for the performance of propeller-powered electric and hybrid aircraft," in *55th AIAA Aerospace Sciences Meeting*. American Institute of Aeronautics and Astronautics, Jan. 2017.

[6] A. Filippone, *Flight Performance of Fixed and Rotary Wing Aircraft*. Butterworth-Heinemann, 2006.

[7] J. Anderson, *Aircraft performance and design*, ser. McGraw-Hill international editions: Aerospace science/technology series. WCB/McGraw-Hill, 1999.

[8] A. R. Hovenburg, T. A. Johansen, and R. Storvold, "Mission performance trade-offs of battery-powered suas," in *2017 International Conference on Unmanned Aerial Systems (ICUAS)*. ICUAS 2017, Jun. 2017.

[9] T. Donateo, A. Ficarella, L. Spedicato, A. Arista, and M. Ferraro, "A new approach to calculating endurance in electric flight and comparing fuel cells and batteries," *Applied Energy*, vol. 187, pp. 807–819, 2017. [Online]. Available: http://dx.doi.org/10.1016/j.apenergy.2016.11.100

[10] L. Traub, "Range and endurance estimates for battery-powered aircraft," *Journal of Aircraft*, pp. 703–707, 2011.

[11] J. Anderson, *Introduction to Flight*, ser. Anderson series - International edition. McGraw-Hill, 2012.

[12] F. J. Hale and A. R. Steiger, "Effects of wind on aircraft cruise performance," in *1978 AIAA Aircraft Systems and Technology Conference*. American Institute of Aeronautics and Astronautics, Aug. 1978.

[13] L. A. Weitz, *Derivation of a Point-Mass Aircraft Model used for Fast-Time Simulation*. MITRE Corporation, 2015.

[14] K. Merical, T. Beechner, and P. Yelvington, "Hybrid-electric, heavy-fuel propulsion system for small unmanned aircraft," *International Journal of Aerospace*, vol. 7, pp. 126–134, 2014.

[15] W. International, "3w-28i hfe fi test data," http://3w-international.com/Drone_Engines_Sale/engine-details-test-data/engine-data-3W-28i-HFE-FI.php, 2016.

[16] M. Coombes, W.-H. Chen, and P. Render, "Reachability analysis of landing sites for forced landing of a uas inwind using trochoidal turn paths matthew," in *2015 International Conference on Unmanned Aerial Systems (ICUAS)*. ICUAS 2017, Jun. 2015.

[17] A. Franco, D. Rivas, and A. Valenzuela, "Optimization of unpowered descents of commercial aircraft in altitude-dependent winds," *Journal of Aircraft*, vol. 49, no. 5, pp. 1460–1470, 2012.

[18] A. Valenzuela and D. Rivas, "Analysis of wind-shear effects on optimal aircraft cruise," *Journal of Guidance, Control and Dynamics*, vol. 39, no. 9, pp. 2148–2155, 9 2016.